Accepted for publication in the Journal of Applied Physics

SAND2016-10421J

Mechanical and optical response of [100] lithium fluoride to multi-megabar dynamic pressures

Jean-Paul Davis[1], Marcus D. Knudson[1,2], Luke Shulenburger[1],

and Scott D. Crockett[3]

[1]Sandia National Laboratories, Albuquerque, New Mexico 87185, USA

[2]Institute for Shock Physics, Washington State University, Pullman, Washington 99164, USA

[3]Los Alamos National Laboratory, Los Alamos, New Mexico 87545, USA

An understanding of the mechanical and optical properties of lithium fluoride (LiF) is essential to its use as a transparent tamper and window for dynamic materials experiments. In order to improve models for this material, we applied iterative Lagrangian analysis to ten independent sets of data from magnetically-driven planar shockless compression experiments on single crystal [100] LiF to pressures as high as 350 GPa. We found that the compression response disagreed with a prevalent tabular equation of state for LiF that is commonly used to interpret shockless compression experiments. We also present complementary data from *ab initio* calculations performed using the diffusion quantum Monte Carlo method. The agreement between these two data sets lends confidence to our interpretation. In order to aid in future experimental analysis, we have modified the tabular EOS to match the new data. We have also extended knowledge of the optical properties of LiF via shock-compression and shockless compression experiments, refining the transmissibility limit, measuring the refractive index to ~300 GPa, and confirming the nonlinear dependence of the refractive index on density. We present a new model for the refractive index of LiF that includes temperature dependence, and describe a procedure for correcting apparent velocity to true velocity for dynamic compression experiments.

I. INTRODUCTION

Single-crystal lithium fluoride (LiF) in the [100] orientation is used extensively in dynamic high pressure experiments as a transparent tamper and optical window for laser-based interferometric velocimetry measurements. At the commonly-used 532-nm wavelength, LiF remains transparent up to around 200 GPa under shock loading[1, 2] and at least 800 GPa under shockless (ramped) loading.[3] While *ab initio* calculations[4] suggest a second solid phase above ~140 GPa and ~3000 K, there is no experimental evidence that crystalline LiF undergoes any stress-driven structural phase transformations. This is important because such phase transformations could complicate LiF's response, both mechanical (compressibility as a function of density) and optical (refractive index as a function of density). These must be well characterized in order to extract information about the shockless mechanical response of a sample under study when LiF is used as an optical window.

The modern Sesame tabular equation of state (EOS) 7271[5] for LiF is often used in part because it is in excellent agreement with the Hugoniot data of Carter[6] (which extend to 108 GPa). Along the principal isentrope, however, shockless compression data to 114 GPa suggest that Sesame 7271 begins to under-predict the compressibility.[7] With the advent of multi-megabar shockless compression techniques using facilities like the Z machine at Sandia National Laboratories or the National Ignition Facility (NIF) at Lawrence Livermore National Laboratory, there is a consequent need for shockless compression measurements on LiF to such high pressures. Section II on the mechanical response of LiF presents a large set of new data on shockless compression of LiF up to 350 GPa, along with a modified tabular EOS to match these data, and Diffusion Quantum Monte Carlo (DMC) results for isentropic compression of LiF that further increase confidence in the new model.

Concerning the optical response of LiF, Rigg *et al*[2] provide an excellent review of previous work measuring and modeling the refractive index as a function of density. While most work in this area has concluded that a linear dependence on density is adequate to describe the refractive index of LiF over a wide range of conditions, the data in Ref. 2 show unequivocally that the dependence on density is non-linear at higher pressure. At least two *ab initio* studies[8, 9] also suggest non-linear dependence. The deviation from linearity leads to decidedly non-negligible differences in inferred velocity for LiF-windowed, multi-megabar experiments. In Sec. III on the optical response of LiF, the results of Ref. 2 are extended by one additional datum at 210 GPa on the Hugoniot, and by a continuous measurement of refractive index under shockless compression to 300 GPa. Then an empirical model is suggested for use in a window correction procedure to obtain true velocity from measured apparent velocity for multi-megabar experiments. Discussion and conclusions are presented in Sec. IV and Sec. V, respectively.

II. MECHANICAL RESPONSE

A. Experimental Method

Shockless compression experiments on LiF were performed using the magnetic ramp-loading technique[10] of the refurbished Z machine[11] at Sandia National Laboratories. The present work considers 10 independent measurements of shockless compression response from seven different shots on Z. All experiments used the narrow stripline short-circuit load detailed elsewhere.[12, 13] Earlier experiments used aluminum 6061-T6 electrodes with cylindrical spot-face features and samples, while later experiments transitioned to rectangular features with square samples. The last two experiments reported here used pure copper electrodes. Figure 1 shows a typical stripline load, and Table I gives configuration details for 11 measurements (the

TABLE I. Configuration details for 11 shockless-compression experiments on LiF.

Experiment	Type	Interface	Features	Anode Thickness		Cathode Thickness	
				Electrode (mm)	Sample (mm)	Electrode (mm)	Sample (mm)
Z1935Top	Single	Free-surface	Round	Al 2.000	—	Al 0.998	1.539
Z1939Bottom	Dual	Windowed	Round	Al 1.002	1.418	Al 1.003	0.916
Z2547Top	Single	Windowed Anode Only	Round	Al 2.003	1.037	Al 2.001	—
Z2547Middle	Single	Windowed Anode Only	Round	Al 2.003	1.384	Al 2.001	—
Z2714Pos3	Single	Windowed	Square	Al 1.195	1.188	Al 1.205	—
Z2756Pos2	Single	Free-surface	Square	Al 3.009	—	Al 1.186	1.724
Z2756Pos3	Single	Windowed	Square	Al 1.197	1.201	Al 1.187	—
Z2756Pos4	Dual	Free-surface	Square	Al 1.197	2.074	Al 1.188	1.731
Z2813Pos1	Single	Free-surface	Square	Cu 1.499	1.785	Cu 1.500	—
Z2813Pos3[a]	N/A	Windowed Anode Only	Square	Cu 1.500	—	Cu 1.502	—
Z2878Top	Single	Free-surface	Square	Cu 0.998	2.023	Cu 0.999	—

a) This experiment was a refractive-index measurement and therefore had no samples.

10 mechanical measurements plus one refractive-index measurement discussed in Sec. III). These experiments include both free-surface and LiF-windowed measurements, as well as single-sample (sample on one electrode and drive measurement on the other) and dual-sample (samples on both electrodes) cases. Time-resolved velocities were measured using a laser-based (532-nm wavelength), fiber-coupled VISAR (Velocity Interferometry System for Any Reflector) technique[14] with fast solid-state photodetectors.

Each measurement consists of two velocity profiles taken from opposite sides of the stripline at the same vertical position. These positions are labeled Top/Middle/Bottom when the stripline contains three positions, and Pos1-Pos4 (from top to bottom) when it contains four positions. For free-surface measurements,

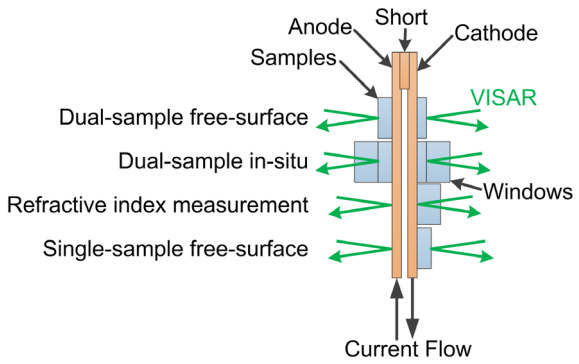

FIG. 1. Notional cross-section view of a stripline showing four experiment configurations (not shown is the single-sample in-situ case).

VISAR measures the true velocity, and the deduced mechanical response is uncoupled from the optical response of LiF. For windowed measurements (which constitute half of the 10 present experiments), however, the measurement of mechanical response is coupled to the optical response. Thus some iteration was involved in arriving at the models suggested in the present work. After averaging and filtering the raw velocity waveforms as described in Ref. 12, final results for the mechanical response used the procedure detailed in Sec. III.B to obtain true velocity for windowed measurements.

B. Analysis

Pairs of velocity profiles were treated by either dual-sample or single-sample iterative Lagrangian analysis (ILA) techniques as detailed in Ref. 12. LiF-windowed measurements of LiF samples give in-material velocities, and do not require the measured-to-in-material velocity mapping step of ILA. Hence iteration is only used to recompute the correction for unequal electrode thicknesses in the dual-sample case, and to recompute the sample input velocity in the single-sample case. For single-sample experiments using square features, any cross-gap non-uniformity of magnetic field beginning prior to the time of peak current was accounted for using 2-D magneto-hydrodynamic (MHD) simulations. For both 1-D (needed as part of single-sample analysis) and 2-D MHD simulations, aluminum electrodes were modeled as described in Ref. 12, while copper electrodes were modeled using the Sandia tabular EOS 3325[15-16] and tabular conductivity 29325,[16] with a standard Steinberg-Guinan rate-independent model[17] for strength.

ILA results, given by Lagrangian wave speed c_L as a function of compression velocity u^*, are presented in Fig. 2 for the 10 experiments and compared to principal isentropes extracted from the Sesame 7271 EOS as well as the modified 7271v3 EOS discussed in Sec. II.C. Individual results have been truncated to discard any unrealistically large systematic deviations

that could be due to reverberation within the sample, free-surface interactions with the sample strength, or other unknown causes. Uncertainties were computed based on experimental measurement uncertainties in timing (±0.1–0.2 ns) and velocity (±10 m/s) per the equations in Ref. 12. These are shown in Fig. 2 only for one measurement, Z1939Bot, which can be considered a worst case; it used a dual-sample configuration and was an older Z shot with higher timing uncertainty than newer shots. It is clear from Fig. 2 that the 7271 EOS is inadequate at multi-megabar pressures along the principal isentrope.

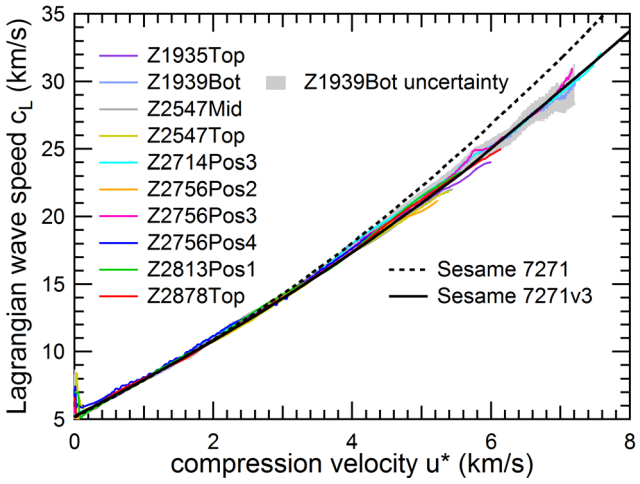

FIG. 2. Results for each of the 10 shockless compression measurements compared to the principal isentropes from tabular EOS 7271 and 7271v3 in wave speed vs. velocity. The worst case uncertainty band is shown for Z1939Bot.

The individual shockless compression results were used to calculate a weighted average and the uncertainty band on that average. These were then integrated to arrive at the average stress-density curve with upper and lower bounds shown in Fig. 3. The uncertainty band is quite narrow, but it does not include any systematic uncertainty in the electrode material models used in single-sample analyses, which comprise eight of the ten experiments averaged here. As discussed in Ref. 12, rigorous quantification of uncertainties due to the use of model standards through MHD simulations in

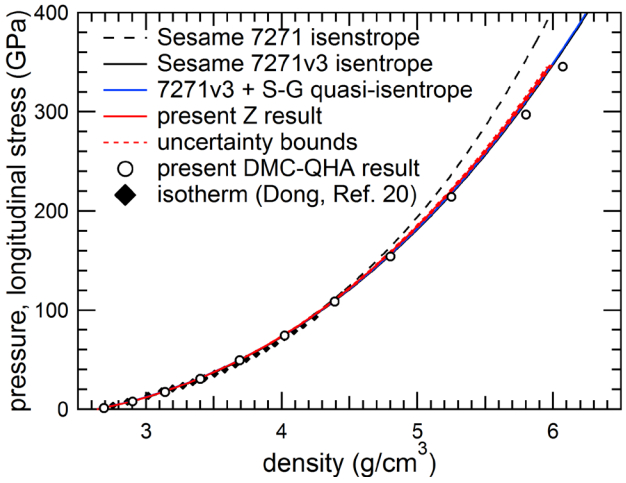

FIG. 3. Average result from Z experiments compared in stress (or pressure) vs. density to the principal isentropes from tabular EOS 7271 and 7271v3, a quasi-isentrope based on 7271v3 and Steinberg-Guinan strength, the present DMC-QHA results, and isotherm data from Ref. 20.

single-sample analysis is a non-trivial problem that has not yet been addressed. Based on previous work on aluminum[18] and copper,[19] uncertainties in the EOS standards are expected to be small, of the order 2–4% in pressure and strain. These errors may partially cancel out as the single-sample input velocity is determined by backward then forward simulations through the electrode. Thus we conservatively estimate systematic uncertainty up to ±1–3% in the averaged experimental result of Fig. 3.

In addition to the pressure-density principal isentropes extracted from Sesame 7271 and 7271v3 tabular EOS, Fig. 3 also shows a stress-density quasi-isentrope extracted from a hydro-code simulation using Sesame 7271v3 and a Steinberg-Guinan (S-G) yield-strength model with parameters as reported in Ref. 7. This is nearly indistinguishable from the principal isentrope at multi-megabar pressures. The strength of LiF at these pressures is dominated by extrapolation of the pressure-hardening found in Ref. 7, and is clearly negligible compared to experimental uncertainties. Finally, Fig. 3 also plots for comparison the Au-standard, diamond-anvil cell, room-temperature isotherm data of Dong *et al*.[20]

Fitting the experimental quasi-isentrope to a higher-order Vinet form as in Ref. 19, where the longitudinal stress σ_x is given as a function of density ρ by

$$\sigma_x(Y) = \frac{3K_0 Y}{(1-Y)^2}\exp\left(aY + bY^2 + cY^3\right) \qquad (1)$$

with $Y = 1-\left(\rho_0/\rho\right)^{1/3}$, yields coefficient values of K_0 = 72.5 ± 0.1 GPa, a = 4.655 ± 0.026, b = 5.59 ± 0.16, and c = −5.38 ± 0.3; errors are one standard deviation. As expected, the quasi-isentropic bulk modulus K_0 is slightly higher than the well-established isothermal bulk modulus value of 66 GPa.[20]

C. Modified Tabular EOS

The tabular equation of state for LiF[5] is based on a standard three-term decomposition of the Helmholtz free energy F with respect to density ρ and temperature T:

$$F(\rho,T) = F_c(\rho,T) + F_i(\rho,T) + F_{el}(\rho,T). \quad (2)$$

The three terms consist of a zero temperature cold curve F_c, an ion thermal component F_i, and an electron thermal component F_{el}. The cold curve term represents the ground state of the electron with the nuclei in fixed equilibrium positions. The ion thermal term represents the thermal motion of the nuclei, modeled here by a Debye approximation for the solid and a corrected Debye approximation for the liquid.[21] The electron thermal term approximates the thermal excitation of the electrons out of the ground state, modeled here by the Thomas-Fermi-Dirac average atom model.[22]

The cold curve was generated using a Mie-Grüneisen approximation with a linear fit to shock-velocity/particle-velocity data[6], U_s=5.215+1.351U_p. The ambient Grüneisen parameter Γ_0 was fixed to the previous value used in the 7271 table, 1.63. The modification made to the EOS to arrive at 7271v3 consisted of a simple change to the derivative of the Grüneisen parameter with respect to the natural log of the density, $d\Gamma/d\ln\rho$. Originally set to −3.2, this was replaced with a value of −1.23 for the 7271v3 table. This modification increases the thermal ion pressure while decreasing the pressure of the cold curve, making it more compressible. The change was required in order to reproduce reasonable sound velocities and the principal isentrope while simultaneously preserving the match to the Hugoniot.

D. *Ab Initio* Calculations

In order to aid in the development of models for the equation of state of LiF, we have augmented our experimental investigations with high fidelity *ab initio* computations of the

equilibrium equation of state of solid LiF under pressure. The Helmholtz free energy is represented by the same decomposition as in Eq. 2, except that the electron thermal contribution F_{el} is neglected due to the large electronic band gap of solid LiF. The cold curve energy F_c was determined using diffusion quantum Monte Carlo calculations, and the ionic free energy F_i was determined via quasi-harmonic phonon calculations within density functional theory.

Diffusion Quantum Monte Carlo (DMC) is a high-fidelity many-body method for solving the Schrödinger equation. We used the open source QMCPACK code[23, 24] to perform DMC calculations of the energy versus volume of pure crystalline LiF in the B1 crystal structure. Previous work showed DMC calculations of the LiF cold curve having properties within 2% of experiment.[25] Subsequent work suggested that the largest approximation to be reduced was due to the pseudopotentials in the calculation.[26] For this reason, we used an all-electron Coulomb treatment of Li and a hard helium core pseudopotential for F. All other details of the calculations concerning convergence of technical parameters and reduction of finite size effects are as reported in Ref 23.

The ionic contribution to the equation of state was determined using the quasi-harmonic approximation (QHA). Density functional theory (DFT) calculations within the local density approximation of 4×4×4 supercells with finite displacements were performed using VASP.[27-29] The force constants from these calculations were analyzed using PHON,[30] resulting in dynamical matrices which are diagonalized to determine the phonon spectrum. From this information, a phonon Helmholtz free energy as a function of temperature was determined at each volume. Then the pressure was calculated by fitting a Vinet EOS[31] to the free energy *vs*. volume curve at the given temperature. Entropies as a function of volume and temperature were also determined from this harmonic Hamiltonian, allowing isentropes to be calculated starting from arbitrary

initial conditions. Points computed on the principal isentrope are plotted in Fig. 3; these show excellent agreement with the present experimental data as well as the 7271v3 tabular EOS, but indicate a slightly more compressible response at ~300 GPa and above.

III. OPTICAL RESPONSE

A. Experiments

To measure the refractive index of LiF under dynamic high pressures requires both the apparent velocity u_a measured through a LiF window (typically using VISAR), and an independent determination of the corresponding true velocity u_t at the LiF front surface. For the impact experiments of Ref. 2, u_t is determined by impedance matching the flyer material to LiF using the known linear relation between shock velocity U_s and particle velocity u_p for each material along with the measured impact velocity u_d, and solving for u_t=u_p of the LiF. Then for a single shock present inside the window, refractive index n is given by[2]

$$n = \frac{n_0 U_S - u_a}{U_S - u_t} \ , \tag{3}$$

where n_0 is the refractive index at ambient conditions.

One shock compression experiment, Z2877, was performed as part of the present study in order to extend the results of Ref. 2. This experiment used the same capability of the Z machine to launch hypervelocity flyer plates,[32, 33] with one minor difference: the electro-deposited copper layer on the flyer's impact surface was thicker than those used in Ref. 2. This delayed overtake of the shock in the LiF by the release wave, allowing a steady shock to propagate through the entire thickness of the LiF and hence providing a transit-time measurement of the shock velocity U_S. Table II summarizes the results of this experiment, including pressure P and

density ρ of the shocked LiF. The measured shock velocity of 13.28 km/s is within uncertainty of the value 13.326 km/s given by the linear U_s–u_p parameters for LiF from the reinterpretation of Carter's[6] data described in Ref. 2. Thus the Carter Hugoniot is accurate to at least 210 GPa, validating its use in Ref. 2 to determine true velocity.

TABLE II. Summarized results of shock experiment Z2877 (u_a and n are specific to λ_0 = 532 nm). Errors in parentheses are one standard deviation.

Impactor	Cu
u_d (km/s)	8.873 (0.02)
U_S (km/s)	13.28 (0.1)
P (GPa)	210.4 (1.2)
ρ (g/cm^3)	4.821 (0.026)
u_a (km/s)	7.8 (0.02)
u_t (km/s)	6.004 (0.017)
n	1.4716 (0.0045)

Another important result from the present shock experiment is that LiF remains transparent at a shock loading of 210 GPa. LiF was shown in Ref. 2 to go opaque at a shock loading of 220 GPa. Thus the interval in shock pressure where LiF's transmissibility limit falls has been narrowed to 210 GPa < P < 220 GPa.

For shockless compression experiments, u_a is measured at the interface of a LiF window bonded directly to the electrode material, and u_t is determined by MHD hydro-code simulations based on a free-surface measurement of the stripline's opposing electrode, using the single-sample ILA procedure as detailed in Ref. 11. For an unsteady compression wave inside the window, it has been shown that refractive index can be expressed as a function of density ρ by the differential equation[34]

$$\frac{dn}{d\rho} = \frac{1}{\rho}\left(n - \frac{du_a}{du_t}\right). \tag{4}$$

The present study includes one shockless compression measurement of refractive index, experiment Z2813Pos3 in Table I. The inverse optimization to determine driving magnetic field, the 2-D MHD simulations to determine cross-gap non-uniformity of magnetic field, and the 1-D simulation to compute u_t all used the models for copper and LiF given in Sec. II.B. To solve Eq. 4, $\rho(u_t)$ was taken along the principal isentrope extracted from the 7271v3 tabular EOS. The result for $n(\rho)$ is shown in Fig. 4 along with the shock-compression datum from Table II and a

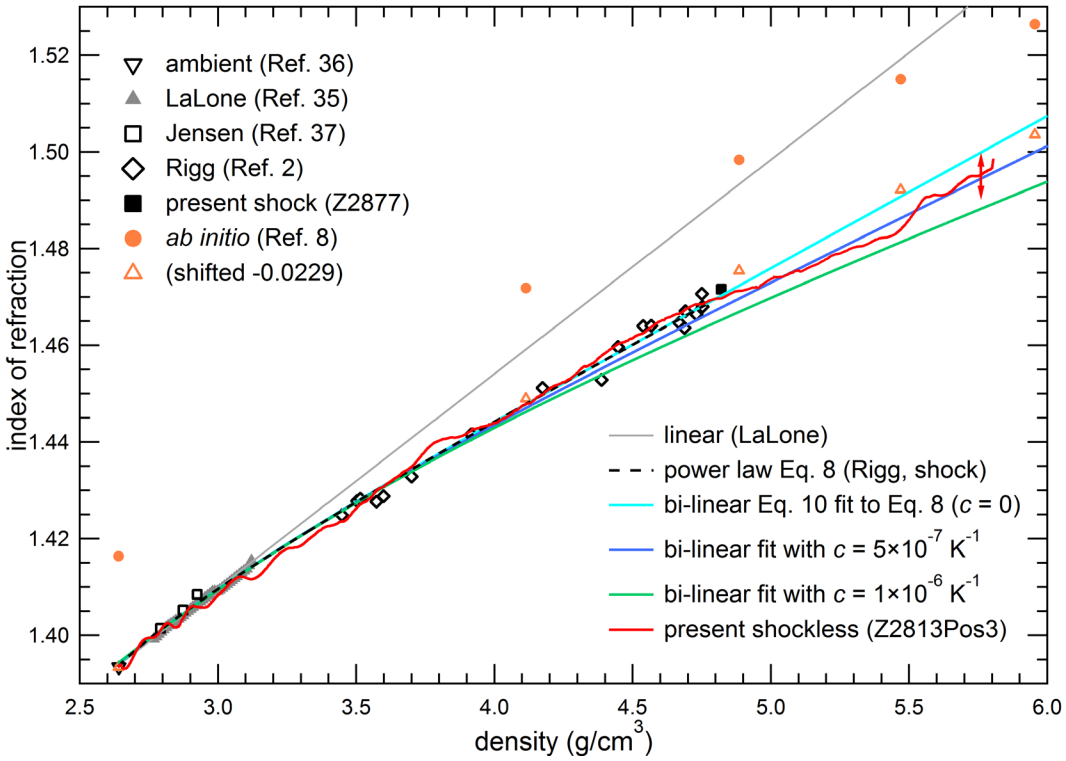

FIG. 4. Measurements and models for refractive index of LiF as a function of density. The vertical red line is a conservative estimate of uncertainty in the shockless index measurement.

collection of shock-compression data[2, 35-37] from the literature. A conservative estimate for uncertainty in the shockless measurement is shown for u_a and u_t having opposite errors of ±10 m/s. Shown for comparison are the *ab initio* results from Ref. 8; these follow the same trend as the shocked and shockless data but with an offset of 0.0229 in refractive index at ambient conditions. The present shockless measurement shows good agreement with the shock data as well as the models presented in Sec. III.C.

B. Window Correction for Shockless Compression

If refractive index is a function only of density and is linear in density, $n = a + b\rho$, then the window correction relating true velocity to apparent velocity is a constant, $u_a = au_t$, regardless of whether the wave in the window is steady or unsteady.[34] For more general $n(\rho)$, and general loading conditions, one can obtain u_t from measured u_a by deconvolving the full

hydrodynamic description of time-dependent spatial distributions of density and velocity inside the window using an iterative approach.[38] For a simple ramped compression wave in the window, Hayes[34] showed the result depends only on window properties as functions of the true interface velocity, thus eliminating the need to compute the full window problem. We prefer, however, to use the more general approach because this allows us to consider temperature dependence of the refractive index, and to account for the formation and growth of shock waves inside the window.

Hydrodynamic simulations of the window rely on the LASLO 1-D code,[39] with a velocity boundary condition at the window input set equal to the true velocity, and using an additional routine to compute the apparent velocity at each time step. For a given function $n(\rho,T)$, this routine calculates

$$u_a = -\frac{dZ}{dt}, \tag{5}$$

where

$$Z = \int_{x_0}^{x_L} n(x)dx \tag{6}$$

is optical path length through the window with driven boundary at position x_0 and undriven boundary at position x_L. An initial guess at u_t is given by applying a linear-index window correction to the measured u_a. Then, after each iteration of the simulation, a new guess at u_t is found by applying the calculated time-dependent window correction factor

$$\psi(t) = \left.\frac{u_t}{u_a}\right|_{calc} \tag{7}$$

to the measured u_a. Convergence is attained when the calculated u_a matches the measured u_a within a specified tolerance. The mechanical response of LiF is represented by the models

described in Sec. II.B (tabular EOS 7271v3 and S-G yield strength). Figure 5 shows an example of the difference between the initial guess and final result for u_t, from a windowed experiment (Z2766Pos1) on copper, using the bi-linear refractive-index model (Eq. 10) described in the next section. The correct true velocity lies about 3% lower than the result assuming a linear-index correction, not insignificant considering the high accuracy of shockless compression data from the Z machine.

C. Refractive Index Model

There have been several forms proposed for the density dependence of refractive index, generally as modifications or extensions to the Gladstone-Dale relation. The shock-compression data on LiF in Ref. 2 was found to be best fit by a form suggested by Wise and Chhabildas,[40]

$$\frac{n-1}{n_0-1}=\frac{1-\gamma\eta^{\kappa}}{1-\eta}, \tag{8}$$

where $\eta = 1 - \rho_0/\rho$ is volumetric strain and the term $\gamma\eta^{\kappa}$ represents departure from Gladstone-Dale; best fit parameters were $\gamma = 0.8051$ and $\kappa = 1.0654$. This curve is shown in Fig. 4.

The apparent velocity corresponding to Fig. 5 exhibits a step at about 3.42 μs (where the true velocity should be smooth), which of course persists in the linear-index correction result. As shown by Brown *et al*,[41] this step is due to the formation of a shock inside the window, suggesting that

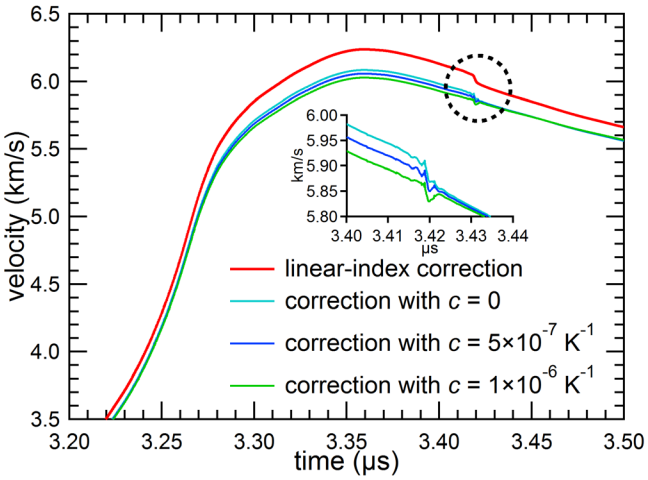

FIG. 5. Example multi-megabar velocity profile (zoomed in to the peak region) comparing the linear-index correction to the full nonlinear-index correction for different temperature coefficients. The dashed-line circle is to draw attention to the step feature due to shock formation in the window, and the inset zooms into the corrected step.

refractive index has some temperature dependence. While the magnitude of the step is sensitive to this temperature dependence, the timing of the step (*i.e.*, the timing of shock formation) is sensitive to the mechanical response of LiF. Thus, through iterative trial and error application of the window correction method detailed in Sec. III.B, we could attempt to infer both the best candidate modified tabular EOS for LiF and the first-order temperature dependence of LiF's refractive index by how well the step is mitigated.

Temperature dependence was taken relative to the refractive index under shockless, or nominally isentropic loading;

$$n = n_{isen} + c\left(T - T_{isen}\right), \tag{9}$$

where T_{isen} is represented by a third-order polynomial in density fit to $T(\rho)$ along the principal isentrope extracted from the 7271v3 tabular EOS. Note that this equation is different than the one used in Ref. 41, and should not necessarily have the same value for c.

Instead of the power-law form of Eq. 8, we adopted the following purely empirical bi-linear form for n_{isen} in order to reproduce more faithfully the linear behavior near ambient conditions:

$$n_{isen} = \frac{a_1 + a_2\rho}{1 + e^{a_3(\rho - a_4)}} + \left(a_5 + a_6\rho\right)\left(1 - \frac{1}{1 + e^{a_3(\rho - a_4)}}\right). \tag{10}$$

This was fit to Eq. 8 adjusted for the difference between Hugoniot and isentrope temperatures using three different values of the temperature coefficient c in Eq. 9: 0, 5×10^{-7}, and 1×10^{-6} K^{-1}. Values for the constants a_1–a_6 are listed in Table III for all three cases, and the resulting curves are shown in Fig. 4. At the

TABLE III. Values for constants in bi-linear refractive index, Eq. 10, for different temperature coefficients.

c (K^{-1})	0	5×10^{-7}	1×10^{-6}
a_1	0.525799	0.611942	0.487427
a_2 (cm^3/g)	0.0149962	0.010808	0.0169664
a_3 (cm^3/g)	2.22922	1.40777	0.889009
a_4 (g/cm^3)	0.539276	-0.219582	-1.26178
a_5	1.31868	1.33411	1.36302
a_6 (cm^3/g)	0.0314645	0.0278761	0.0220458

highest pressures, the case of $c = 5\times10^{-7}$ K^{-1} appears most consistent with the shockless measurement of refractive index (experiment Z2813Pos3). Figure 5, however, suggests that $c = 1\times10^{-6}$ K^{-1} works best for mitigating the step due to shock formation inside the window. Therefore, although the present experiments strongly suggest there is a temperature dependence (due to the remaining step for the case $c = 0$ in Fig. 5), they cannot constrain c to better than 0.5–1.0×10^{-6} K^{-1}. Further refinement would require refractive index measurements on pre-heated LiF samples. All present analyses of LiF-windowed data in Fig. 2 and Fig. 6 used Eq. 10 fit to the case of $c = 5\times10^{-7}$ K^{-1}, because the only data of concern occurred well prior to any shock formation in the window.

IV. DISCUSSION

We are suggesting that shockless experiments with LiF windows use the procedure in Sec. III.B with Eq. 10 and the Sesame 7271v3 tabular EOS to deduce true velocity from measured apparent velocity. Confidence in this approach can be gained by comparing measurements of the same material taken with and without windows. This is done in Fig. 6 for measurements on copper. The free-surface measurement from Z2791Pos1-2[19] is compared to a LiF-windowed measurement from Z2766Pos1 in the wave-speed/compression-velocity plane. Also shown is the reference model for copper consisting of Sesame 3325 and Steinberg-Guinan yield strength. The excellent

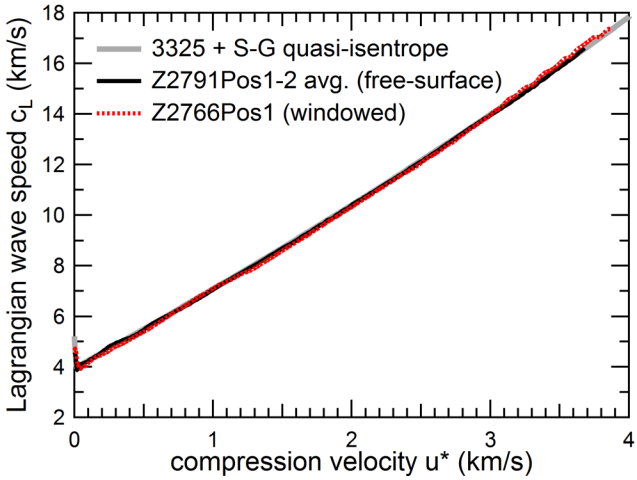

FIG. 6. Two independent measurements of the principal quasi-isentrope of copper, one without windows (Ref. 19) and one with LiF windows, compared to the reference model for copper (Sesame 3325 plus strength).

agreement between all three curves to ~350 GPa (driven side of copper) suggests that the present mechanical and optical models for LiF are accurate to at least ~200 GPa (copper/LiF interface stress) under shockless compression.

The present result for density dependence of refractive index contradicts that of Frantanduono *et al*[3] which showed an approximately linear density dependence under shockless compression to ~800 GPa. In that work, however, true velocity was obtained by impedance matching diamond to LiF assuming the LiF mechanical response could be represented by the original Sesame EOS 7271. The density in Eq. 4 also came from table 7271. In fact, we have shown that table 7271 is too stiff along the principal isentrope. If the 800-GPa data were re-analyzed using the more compressible 7271v3, one would likely see a non-linear density dependence (specifically, higher density for a given refractive index). Though beyond the scope of the present work, this exercise would be well worth undertaking.

Finally, we note that the measured optical response under shockless compression presented here comes from only a single experiment. The result of this experiment agrees well with the refractive index model that was used to analyze the five coupled mechanical/optical measurements; the consistency between these and the purely mechanical measurements increases confidence in the single measurement of refractive index. In the interest of prudence, however, we plan to repeat the experiment in order to ensure reproducibility.

V. CONCLUSION

We applied ILA to measurements taken from ten independent experiments on shockless compression of LiF to multi-megabar pressures that used stripline loads on the Z machine. These included five free-surface measurements, for which the deduced mechanical response is decoupled from optical response, and five windowed measurements, for which the mechanical

and optical responses are coupled. The latter were analyzed using a model for refractive index based on shock compression results adjusted for the temperature difference between shock and shockless compression. The resulting response of LiF in stress-density, measured to ~350 GPa, begins to exhibit compressibility greater than that of the widely used Sesame 7271 tabular EOS for pressures greater than ~100 GPa. We modified the 7271 table by adjusting the density derivative of the Grüneisen parameter to match the shockless data while maintaining agreement with shock data; this 7271v3 table is recommended for future work. For comparison, we performed *ab initio* calculations using DMC for the cold curve and DFT-QHA for the ionic contribution at selected points along the principal isentrope; these showed good agreement with the shockless data.

We performed a shock experiment on LiF at 210 GPa, extending the refractive-index data in Ref. 2 while also validating the Hugoniot model used in that work and refining the pressure range in which LiF's transmissibility limit falls. Another experiment directly measured the refractive index of LiF to ~300 GPa by assuming known mechanical response for copper and LiF; the result compares well to the refractive-index models considered here and re-emphasizes the importance of accounting for non-linear density dependence when deducing true velocity from interferometric velocimetry of LiF-windowed samples under multi-megabar compression. Finally, we outlined a procedure for correcting measured apparent velocity to true velocity using the present models for LiF's mechanical and optical responses.

ACKNOWLEDGEMENTS

The authors wish to acknowledge the support of the large inter-disciplinary team it takes to design, fabricate, and execute experiments on the Z machine. Sandia National Laboratories is a multi-mission laboratory managed and operated by Sandia Corporation, a wholly owned

subsidiary of Lockheed Martin Corporation, for the U.S. Department of Energy's National Nuclear Security Administration under contract DE-AC04-94AL85000. Los Alamos National Laboratory, an affirmative action/equal opportunity employer, is operated by Los Alamos National Security, LLC, for the National Nuclear Security Administration of the U.S. Department of Energy under Contract No. DE-AC52-06NA25396.

REFERENCES

[1] M. D. Furnish, L. C. Chhabildas and W. D. Reinhart, Int. J. Impact Eng. **23**, 261 (1999).

[2] P. A. Rigg, M. D. Knudson, R. J. Scharff and R. S. Hixson, J. Appl. Phys. **116**, 033515 (2014).

[3] D. E. Fratanduono, T. R. Boehly, M. A. Barrios, D. D. Meyerhofer, J. H. Eggert, R. F. Smith, D. G. Hicks, P. M. Celliers, D. G. Braun and G. W. Collins, J. Appl. Phys. **109**, 123521 (2011).

[4] N. A. Smirnov, Phys. Rev. B **83**, 014109 (2011).

[5] S. Crockett and S. Rudin, Los Alamos National Laboratory Report No. LA-UR-06-8401, 2006.

[6] W. J. Carter, High Temp.-High Press. **5**, 313 (1973).

[7] T. Ao, M. D. Knudson, J. R. Asay and J.-P. Davis, J. Appl. Phys. **106**, 103507 (2009).

[8] C. D. Spataru, L. Shulenburger and L. X. Benedict, Phys. Rev. B **92**, 245117 (2015).

[9] Z.-H. Sun, J. Dong and Y.-W. Xia, Physica B: Condensed Matter **406**, 3660 (2011).

[10] C. A. Hall, J. R. Asay, M. D. Knudson, W. A. Stygar, R. B. Spielman, T. D. Pointon, D. B. Reisman, A. Toor and R. C. Cauble, Rev. Sci. Instrum. **72**, 3587 (2001).

[11] M. E. Savage, K. R. LeChien, M. R. Lopez, B. S. Stoltzfus, W. A. Stygar, D. S. Artery, J. A. Lott and P. A. Corcoran, in *Pulsed Power Conference (PPC), 2011 IEEE*, Chicago, IL, USA, 19-23 June 2011 (IEEE, Piscataway, NJ, USA, 2011), pp. 983-990.

[12] J.-P. Davis, J. L. Brown, M. D. Knudson and R. W. Lemke, J. Appl. Phys. **116**, 204903 (2014).

[13] R. W. Lemke, M. D. Knudson and J.-P. Davis, Int. J. Impact Eng. **38**, 480 (2011).

[14] W. F. Hemsing, Rev. Sci. Instrum. **50**, 73 (1979).

[15] John H. Carpenter, private communication

[16] K. R. Cochrane, R. W. Lemke, Z. Riford and J. H. Carpenter, J. Appl. Phys. **119**, 105902 (2016).

[17] D. J. Steinberg, S. G. Cochran and M. W. Guinan, J. Appl. Phys. **51**, 1498 (1980).

[18] J.-P. Davis, J. Appl. Phys. **99**, 103512 (2006).

[19] R. G. Kraus, J.-P. Davis, C. T. Seagle, D. E. Fratanduono, D. C. Swift, J. L. Brown and J. H. Eggert, Phys. Rev. B **93**, 134105 (2016).

[20] H. Dong, S. M. Dorfman, C. M. Holl, Y. Meng, V. B. Prakapenka, D. He and T. S. Duffy, High Pressure Research **34**, 39 (2014).

[21] J. D. Johnson, High Pressure Research **6**, 277 (1991).

[22] S. P. Lyon and J. D. Johnson, Los Alamos National Laboratory Report No. LA-UR-92-3407, 1992, available at http://library.lanl.gov/cgi-bin/getfile?00612717.pdf.

[23] J. Kim, K. P. Esler, J. McMinis, M. A. Morales, B. K. Clark, L. Shulenburger and D. M. Ceperley, J. Phys., Conf. Ser. **402**, 012008 (2012).

[24] K. P. Esler, J. Kim, D. M. Ceperley and L. Shulenburger, Computing in Science & Engineering **14**, 40 (2012).

[25] L. Shulenburger and T. R. Mattsson, Phys. Rev. B **88**, 245117 (2013).

[26] L. Shulenburger, T. R. Mattsson and M. P. Desjarlais, arXiv:1501.03850 (2015).

[27] G. Kresse and J. Hafner, Phys. Rev. B **47**, 558 (1993).

[28] G. Kresse and J. Hafner, Phys. Rev. B **49**, 14251 (1994).

[29] G. Kresse and J. Furthmüller, Phys. Rev. B **54**, 11169 (1996).

[30] D. Alfè, Comput. Phys. Commun. **180**, 2622 (2009).

[31] P. Vinet, J. Ferrante, J. R. Smith and J. H. Rose, Journal of Physics C: Solid State Physics **19**, L467 (1986).

[32] R. W. Lemke, M. D. Knudson, C. A. Hall, T. A. Haill, P. M. Desjarlais, J. R. Asay and T. A. Mehlhorn, Phys. Plasmas **10**, 1092 (2003).

[33] R. W. Lemke, M. D. Knudson, A. C. Robinson, T. A. Haill, K. W. Struve, J. R. Asay and T. A. Mehlhorn, Phys. Plasmas **10**, 1867 (2003).

[34] D. B. Hayes, J. Appl. Phys. **89**, 6484 (2001).

[35] B. M. LaLone, O. V. Fat'yanov, J. R. Asay and Y. M. Gupta, J. Appl. Phys. **103**, 093505 (2008).

[36] B. J. Jensen, D. B. Holtkamp, P. A. Rigg and D. H. Dolan, J. Appl. Phys. **106**, 049901 (2009).

[37] B. J. Jensen, D. B. Holtkamp, P. A. Rigg and D. H. Dolan, J. Appl. Phys. **101**, 013523 (2007).

[38] J. Wackerle, H. L. Stacy and J. C. Dallman, in *SPIE Vol. 832 High Speed Photography, Videography and Photonics V* (1988), pp. 72-82.

[39] Joshua Robbins (personal communication, 2013)

[40] J. L. Wise and L. C. Chhabildas, in *Shock Waves in Condensed Matter*, edited by Y. M. Gupta (Springer US, Boston, MA, 1986), pp. 441-454.

[41] J. L. Brown, C. S. Alexander, J. R. Asay, T. J. Vogler, D. H. Dolan and J. L. Belof, J. Appl. Phys. **115**, 043530 (2014).